scientific reports

Check for updates

OPEN

Analysis of lateral soil displacements induced by synchronous grouting in large-diameter shield tunnelling: a case study

Sige Peng[1], Haobin Huang[2,3], Hong Pan[3,4]✉, Guanyong Luo[3,4]✉ & Hong Cao[3,4]

Soil displacement during underground tunnel construction has become a focal concern in recent decades. Numerous seismic events have revealed that many large deformation of the ground surface was due to underground tunnel construction, especially for the large-diameter shield tunnelling. Evaluating the impact of shield tunneling on surrounding soil requires an in-depth analysis of the extent, magnitude, and primary zones of disturbance caused by synchronous grouting at the shield machine tail. This study, based on a case involving short-range, high-frequency field monitoring during large-diameter shield tunnel construction, presents an incremental displacement method and maximum incremental displacement method to assess the patterns of lateral horizontal soil displacements induced by synchronous grouting. Results indicate a V-shaped displacement distribution in the longitudinal direction, with the disturbance zone extending approximately 1D (equal to the shield's outer diameter). The inclination angle of the boundary was observed to correlate with soil properties. In the lateral direction, disturbances were concentrated just above the tunnel shoulder, with a width of approximately 0.7D, shifting upward as the depth of overlying soil increased. The inclination angle transitioned from shallow to steep within a symmetrical disturbance zone across both sides of the tunnel. Additionally, similar displacement patterns were confirmed in other cases using the maximum incremental displacement method, with an analysis of deformation modes and underlying causes of lateral soil upward movement.

Keywords Large-diameter shield tunnel, Synchronous grouting, Lateral horizontal displacements, Incremental displacement method

The shield method has been extensively used in various types of underground tunnel construction due to its advantages, such as a high degree of mechanization and minimal impact on the surrounding population's living environment. Large-diameter underground tunnel construction poses a grave threat to the ground building structures[1–3], for which it is a key infrastructure for human safety. However, as a key infrastructure for humanity, underground tunnels offer many positive economic, environmental and social dimensions. Therefore, these tunnels tend to cover extensive distances, making it inevitable that many projects intersect with large-diameter shield tunnelling. As tunnels crossing ground building structures will be found often, for it is apparent that a better understanding of the soil displacements induced by construction of large-diameter shield tunnelling is undergoing the urgent need[4–6]. During shield tunnel construction, synchronous grouting is performed at the tail of the shield machine to fill the gap between the machine's shell and the segment structure. This process, known as synchronous grouting, can significantly disturb the surrounding soil. Refining this process could better protect the structures around the tunnel lining, reducing the impact during operation and minimizing the risks associated with shield construction. Therefore, understanding the characteristics of synchronous grouting

[1]School of Civil and Transportation Engineering, Guangdong University of Technology, Guangzhou 510006, China. [2]Poly South China Holdings Co.,Ltd, Foshan 528200, China. [3]School of Civil Engineering and Transportation, South China University of Technology, Guangzhou 510640, China. [4]State Key Laboratory of Subtropical Building Science, South China University of Technology, Guangzhou 510640, China. ✉email: hpan@scut.edu.cn; luogy@scut.edu.cn

and the mechanisms behind the disturbance of the surrounding strata caused by shield tunnelling is crucial for engineering practice.

Several methods are commonly used to evaluate ground deformation caused by shield construction, including: (1) field measurements, such as empirical approaches based on Peck's theory[7] and other fitting models[8], which are typically derived from field data; (2) laboratory tests[9–12]; (3) theoretical analyses[13–15]; and 4) numerical simulations[16–20]. Ground deformation is influenced by various factors, including the mechanisms and kinematic behaviour of the tunnel boring machine (TBM), TBM operational parameters, and geological conditions[21]. This complexity makes it challenging to determine key parameters for empirical and theoretical analyses in advance, which are often obtained through inverse analysis of field measurement data[22–24]. Finite element method (FEM) models often require adjustment based on comparisons with field data[25–27]. Therefore, field measurements are crucial for interpreting the actual ground response during tunnelling, and the analysis of this data provides valuable insights for validating empirical, numerical, and theoretical methods.

Regarding the field measurement methods, analyzing the longitudinal effects of tunnelling parameters and ground displacements during synchronous grouting will enhance the validation of current prediction models. Most existing theoretical solutions are derived under plane strain conditions[28,29] and typically employ displacement-controlled boundary conditions for the tunnel cavity. These solutions often rely on the gap parameter[30,31]. However, the gap parameter is typically computed based solely on the tunnelling parameters at the control section, without accounting for the influence of tunnelling parameters before or after the tunnel advances through this section. In other words, the longitudinal effects of tunnelling parameters are not considered. Cao et al. addressed this limitation by incorporating the longitudinal effects of face pressure and tail grouting[32], modifying the gap parameter formula[31]. Given the importance of understanding the longitudinal effects of tunnelling parameters, it is essential to analyze field-measured data, taking into account the characteristics of longitudinal ground deformations, including their magnitude and distribution, and to establish correlations between ground deformation and tunnelling parameters.

Based on the preceding discussion that the effect of shield synchronous grouting on surrounding soil displacements has not been thoroughly investigated. Without detailed analysis, the underlying mechanisms—such as soil arching, stress redistribution, and changes in pore pressure—remain unclear. These factors could critically influence how the soil responds to the grouting process. The absence of comprehensive studies hampers the development of accurate predictive models for soil behavior during shield tunneling. This could lead to discrepancies between theoretical expectations and actual field performance. Understanding the precise impact of synchronous grouting is essential for optimizing grouting strategies, improving tunnel stability, and reducing potential ground settlements or lateral displacements during construction. This study proposes and evaluates a monitoring scheme for measuring lateral horizontal displacements around the shield machine tail of a large-diameter shield tunnel project in Guangzhou. The monitoring points were positioned in close proximity to the tunnel (with a minimum distance of only 2.1 m) and recorded at high frequency (once per ring as the shield machine advanced). The results highlight the disturbance induced by synchronous grouting and provide insight into the lateral horizontal displacement patterns. The displacement increments and their maximums were analyzed using the displacement increment method and the displacement increment maximums method to characterize the soil response around the shield machine tail.

Case background

This study focuses on a large-diameter shield tunnel constructed in soft soil conditions in Guangzhou, China (Fig. 1), utilizing a slurry shield machine. The slurry shield used in the project had an overall length of approximately 12.4 m, with outer diameters of 11.71 m at the cutter head and 11.66 m at the shield machine tail. The tunnel crown was buried at depths ranging from 11.5 to 17 m, with the shield machine passing beneath roads, residential areas, and fish ponds along the alignment. The geological profile of the monitored section, shown in Fig. 2, indicates that the tunnel primarily traversed layers of sludge and silty clay. In the monitored section, the tunnel crown was buried at a depth of 14.5 m, with the tunnel axis located 20.4 m below the surface. The soil properties of the site are detailed in Table 1.

The gap between the surrounding strata and the tunnel lining was filled with cement grout injected through four grouting ports at the tail of the shield machine during excavation, a process known as synchronous grouting. The locations of the four grouting ports are illustrated in Fig. 3, along with the layout of the inclinometer tubes installed in the monitored section. Lateral horizontal displacements of the surrounding soil were measured using four inclinometer tubes (No. 1 to No. 4) positioned on both sides of the tunnel. As the cutter head approached the reference zero point, the distance was denoted as negative, and once the cutter head passed the monitored section, the distance was considered positive. Measurements began when the cutter head was 33.8 m away from the monitored section and continued until it was 106.3 m beyond it. Since the focus of this study was on the effects of synchronous grouting, the analysis primarily relied on data collected when the cutter head was located between 0 and 34 m behind the monitored section.

The tilt angles of the inclinometers were measured at 0.5 m vertical intervals with a resolution of 0.005 mm and an accuracy of ± 0.003°. Measurements were taken once per ring (2 m) as the cutter head approached the monitored section, continuing until the shield machine tail was 6 m past the monitored point, at which point the frequency was reduced to once every two rings (4 m). The interval between two consecutive measurements was defined as a construction step, and the displacement occurring within each step was classified as the displacement increment in this study.

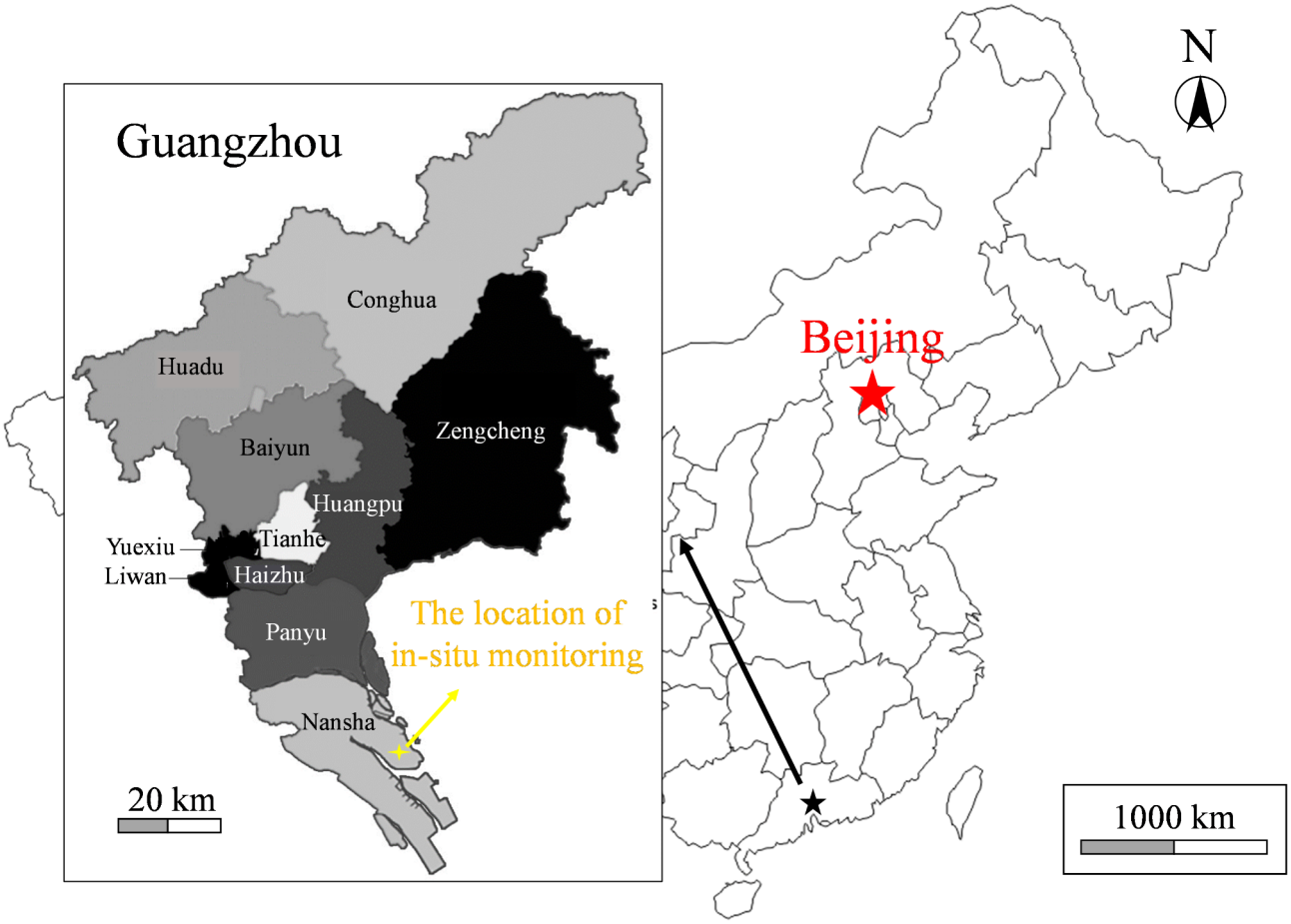

Fig. 1. Location of the Guangzhou tunnel case. Generated using AutoCAD 2020.

Evaluation of lateral horizontal displacements

Lateral horizontal displacements

The lateral horizontal displacements on both sides with respect to the shield machine advancement were illustrated in Fig. 4. The displacements can be divided into three main stages, with respect to the position toward the monitored section, which can be described as follows:

Phase 1 (prior to the arrival of the cutter head, -33.8 m to 0 m): In the initial stage, as the shield machine advanced from a considerable distance (-33.8 m) until the cutter head reached the monitored section, the lateral horizontal displacements of the soil remained minimal, with a maximum deformation of only 4.61 mm.

Phase 2 (between the cutter head pass and the shield machine tail pass, 0–12.3 m): During this phase, the lateral horizontal displacements increased significantly, with the soil primarily deforming away from the tunnel. The maximum deformation exceeded 10 mm and occurred at a point slightly above the tunnel shoulder.

Phase 3 (after the shield machine tail pass, 12.3–106.3 m): Following the shield machine tail pass, the lateral horizontal displacements of the surrounding soil continued to increase due to synchronous grouting, reaching a maximum of approximately 30 mm before stabilizing.

The lateral horizontal displacements on both sides of the tunnel were generally symmetrical, but slightly larger for the right side in comparison to the left, as shown in Fig. 4. The observations from the three inclinometer tubes located on the right side of the tunnel indicated that the lateral horizontal displacements of the soil were relatively small at greater horizontal distances from the tunnel, but soil disturbances at larger distances had a trend to propagate vertically, with occurring the greatest disturbance relatively close to the ground surface. It is obvious that the synchronous grouting during the excavation process has a major influence on the surrounding soil on the shield machine tail arrival and departure stages. However, the total displacements represented the accumulated soil deformations during the construction process, but the soil deformation at each construction step and the effect of synchronous grouting could not be clearly recognized. Therefore, the collected data required further analysis, which was conducted by using the displacement increments method as follows.

Lateral horizontal incremental displacements

The incremental displacements could reveal the effect of each construction step on the surrounding soil and could avoid the cumulative impact caused by the previous construction steps. Although the previous steps could have an influence on the total lateral horizontal displacements, the main concern in this study is to investigate

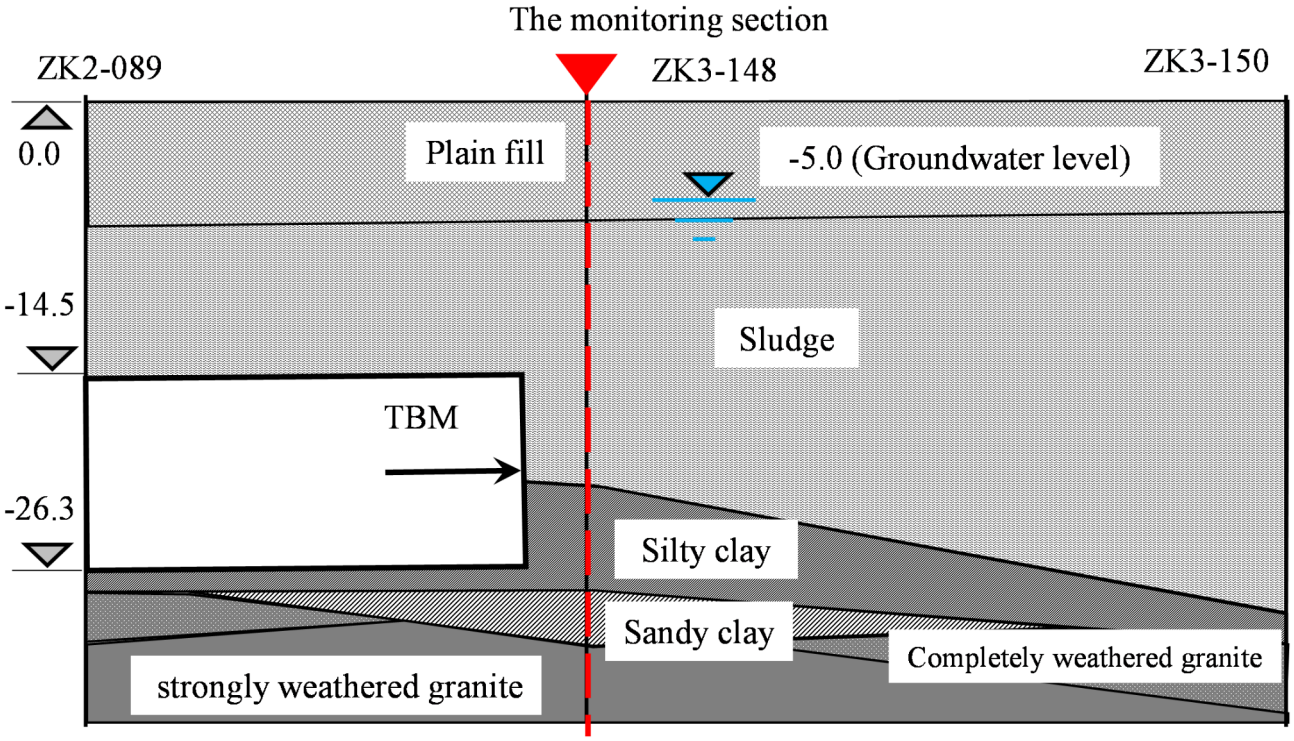

Fig. 2. Longitudinal geology profile of section (unit: m). Generated using AutoCAD 2020.

Soil type	Moisture content W (%)	Unit weight γ (kN/m^3)	Straight direct shear test	
			Cohesion c (kPa)	Internal friction angle φ (°)
Plain fill	/	18.5	5.0	15.0
Sludge	62.4	15.8	8.0	7.0
Silty clay	31.8	18.8	19.8	16.5
Sandy clay	25.5	19.0	25.2	26.5
Completely decomposed mixed granite	23.6	19.2	28.0	29.5

Table 1. Geotechnical properties.

the effect of shield construction during the stage of synchronous grouting. Therefore, the displacement increments method was used to evaluate the disturbance of the surrounding soil for each construction step during synchronous grouting without considering the cumulative impact. Figures 5, 6, 7 and 8 depict the lateral horizontal displacement increment profiles for the four inclinometer tubes (No. 1 to No. 4). Each curve represents the incremental lateral displacement of the soil recorded by the corresponding inclinometer at each construction stage. The red solid line in each figure marks the zero-displacement reference. Displacement incremental curves on the left of this line indicate soil movement toward the tunnel, whereas those on the right indicate movement away from the tunnel.

The above four consecutive figures indicated that the lateral horizontal displacement increments of the soil surrounding the tunnel were relatively large when the shield machine tail was approximately 5 m away from the monitored section, both during the shield machine tail's arrival and departure stages (where the cutter head located approximately 8 m and 18 m ahead of the monitored section, respectively). Most incremental displacements exhibited an outward propagation trend, with inclinometer tube No. 2 recording the largest movement. The maximum displacement increment, 7.64 mm, occurred at a depth of 16 m when the cutter head was 16.28 m ahead of the monitored section. The greatest lateral horizontal deformation for each tube was observed in the upper section of the tunnel or slightly above the tunnel crown, in proximity to the shield machine tail's grouting hole depth. This indicates that synchronous grouting significantly influenced the surrounding soil disturbance. As excavation progressed, the lateral horizontal displacement increments of the surrounding soil increased significantly when in relatively close proximity to the shield machine tail, followed by a slight increase as the shield machine tail moved farther away. This revealed that the magnitude of soil disturbance intensified around the shield machine tail but diminished as the distance increased. In terms of depth, larger disturbances

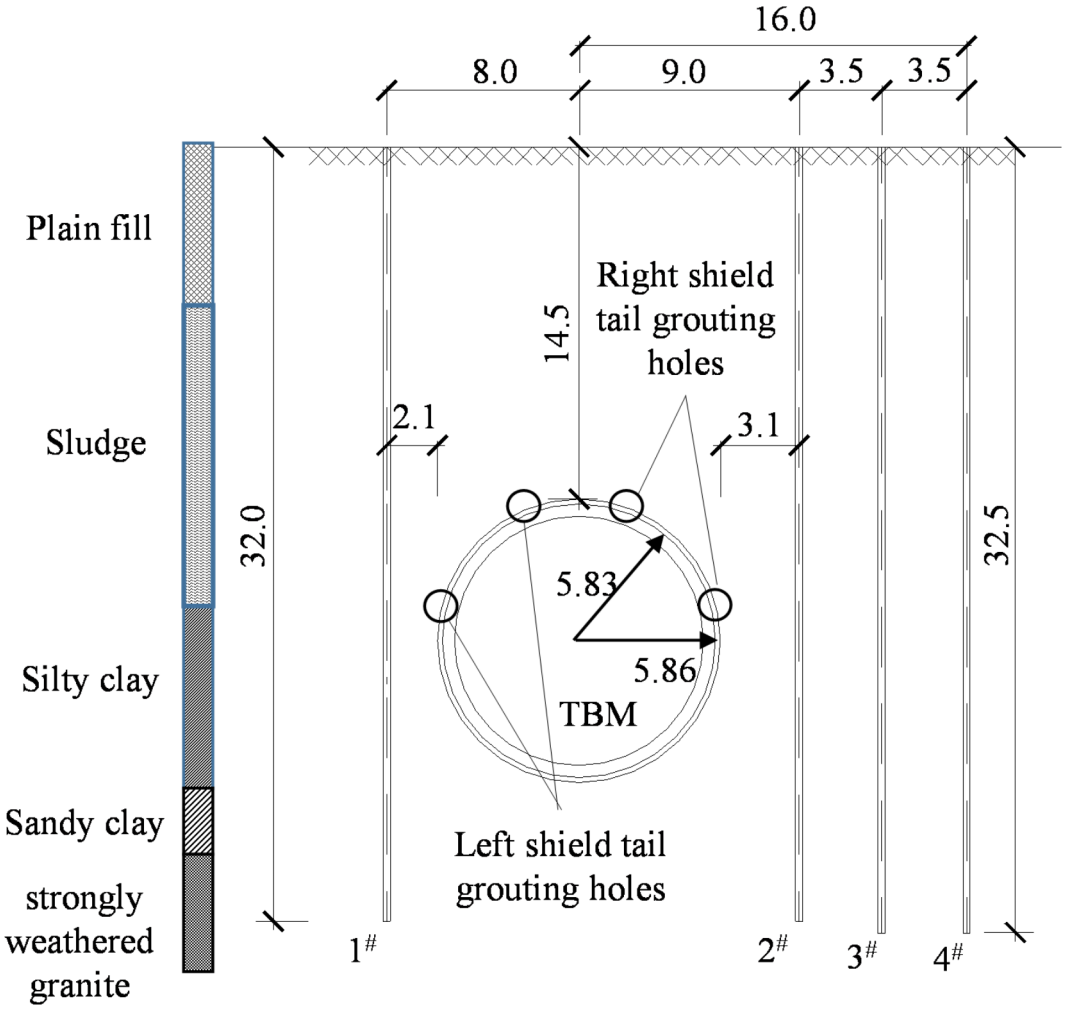

Fig. 3. Layout of monitoring instruments (unit: m). Generated using AutoCAD 2020.

tended to occur at greater depths rather than in shallower areas, with the maximum displacement increments typically observed at deeper positions.

As shown in Fig. 5 for tube No. 1 (located on the left side of the tunnel, see Fig. 4), the lateral horizontal displacements at most measurement points exhibited an outward movement from the tunnel. These displacements were relatively large when the cutter head was 4–18 m ahead of the monitored section. The points with the most significant incremental displacements were concentrated near the full cross-section of the shield tunnel and slightly above its crown. As the excavation advanced, the maximum incremental displacement was initially observed at the tunnel crown when the cutter head passed the monitored section. It then gradually shifted downward as the shield machine tail approached. Upon the shield machine tail reaching the monitored section, this point dropped to the tunnel axis depth, where it stabilized and remained constant for a period, indicating an equilibrium state. Subsequently, as the shield machine tail moved further ahead and the distance to the monitored section increased, the maximum incremental displacement gradually shifted upward toward the surface, eventually reaching the ground surface, where the incremental displacements became negligible. It is noteworthy that some incremental displacements in Fig. 5 exhibited an inward direction toward the tunnel, as illustrated by the incremental displacement curves when the cutter head was positioned 22 m and 30–36 m ahead of the monitored section. A separate analysis was performed on the grout pressures and grout volumes associated with synchronous grouting, revealing that the grout pressures in this area were relatively low, with the pressures at the shield machine tail segment being below 0.305 MPa—this threshold was established prior to construction (as depicted in Fig. 9). This phenomenon was also observed in the data analysis conducted using inclinometer tubes No. 2 through No. 4.

For the other three measurement tubes (No. 2 to No. 4) located on the right side of the tunnel (see Fig. 4), the results showed that the displacement trends were similar to those of tube No. 1, including the direction and magnitude of the lateral horizontal displacements, as illustrated in Figs. 6, 7 and 8. Although tube No. 1 was positioned closer to the tunnel than tube No. 2, its lateral horizontal incremental displacement was smaller than that of tube No. 2 after the shield machine tail passed through the monitored section. This difference may be attributed to the effect of grout pressures. When the tube-to-tunnel distance was constant, the grout pressures

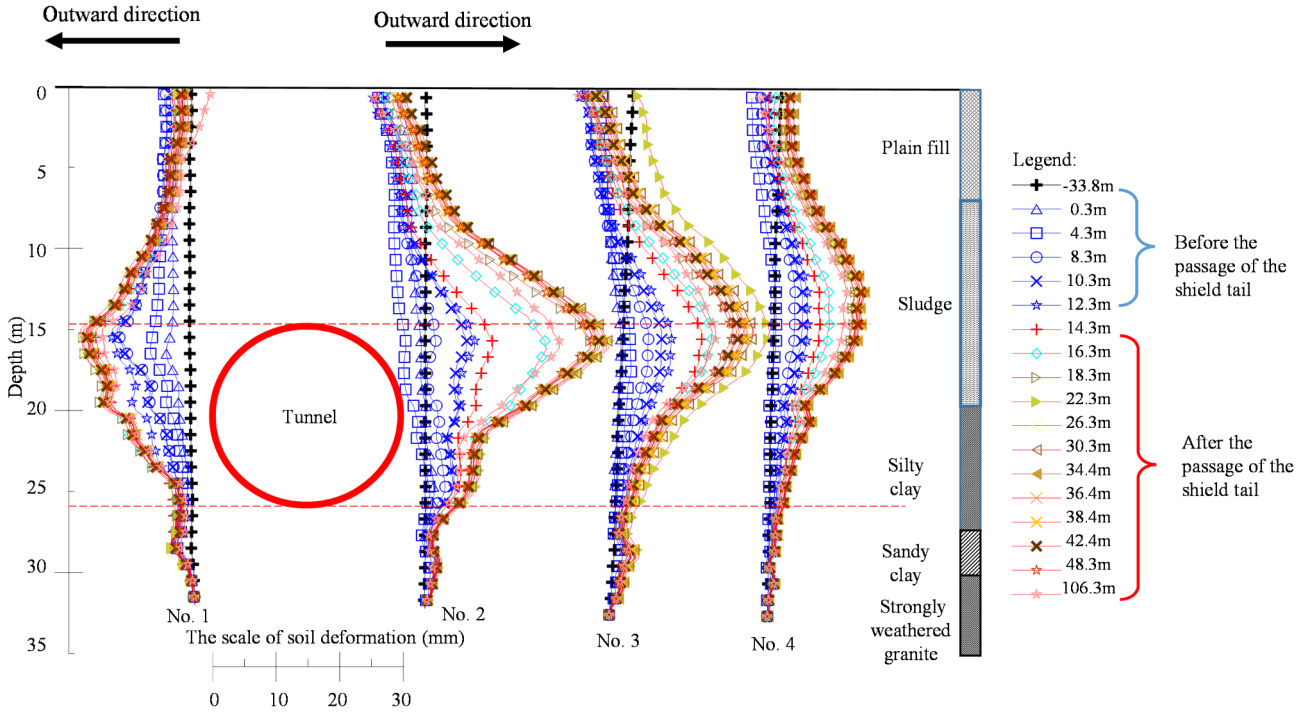

Fig. 4. Lateral horizontal displacements of soil during shield construction. Generated using Grapher 18.

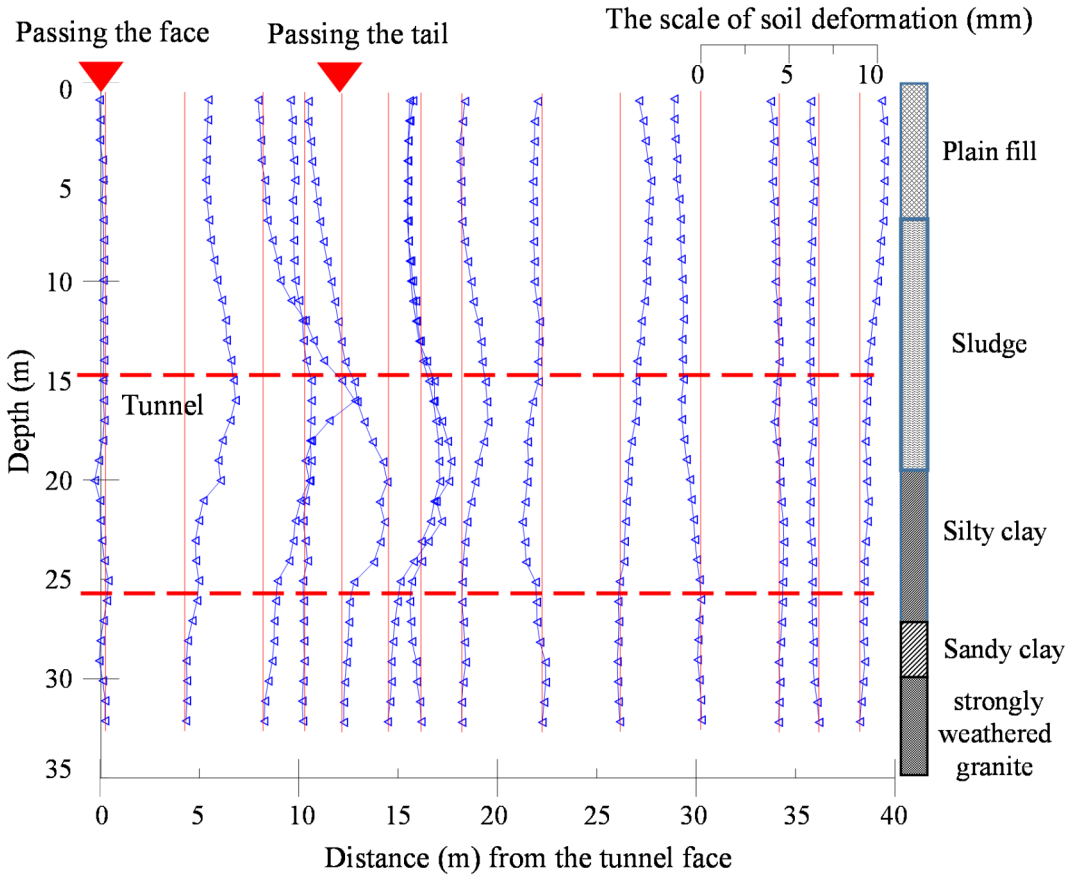

Fig. 5. Lateral horizontal displacement increments at inclinometer tube No. 1. Generated using Grapher 18.

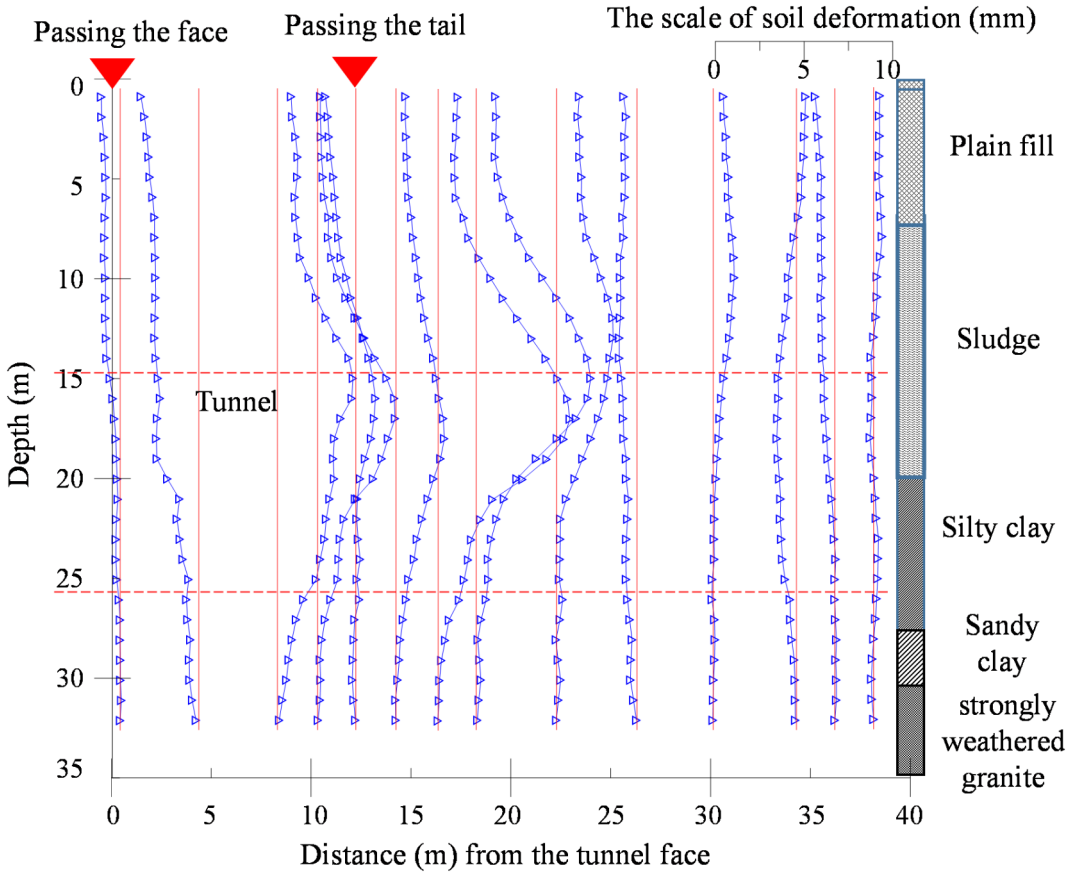

Fig. 6. Lateral horizontal displacement increments at inclinometer tube No. 2. Generated using Grapher 18.

on the right side of the tunnel were generally higher than those on the left, as illustrated in Fig. 9. Additionally, while the grout volumes at most injection points on the right side were relatively higher than those on the left, possibly influencing the lateral horizontal incremental displacement, but the grout volumes were actually larger on the left side than on the right at the range of 0–20 m. This provides further evidence that grout pressures play a significant role in determining lateral horizontal incremental displacement, even when grout volumes vary considerably. Moreover, the regions with larger incremental displacements for all the tubes were generally concentrated between the tunnel axis and slightly above the tunnel crown, although the displacement zones for tubes No. 2–No. 4 were shallower than that of tube No. 1. As the distance between the inclinometer tube and the tunnel increased, the regions of larger lateral horizontal displacement increments shifted to shallower positions, and the incremental displacements became smaller.

Compared to using lateral horizontal displacements, incremental displacement proved to be more effective in identifying the displacement patterns of the surrounding soil during the grouting process. However, due to the dynamic and complex nature of TBM control parameters in shield tunnelling, the magnitude of incremental displacements is influenced by multiple factors. To further analyse the lateral horizontal disturbances to the surrounding soil caused by synchronous grouting at the shield machine tail, the primary disturbance zone was identified by examining the depths of maximum increments at the four inclinometer tubes. Once the major disturbance zone caused by synchronous grouting was determined, the surrounding soil disturbance could be effectively managed by ensuring that the maximum value within this disturbance zone remains within acceptable safety limits.

Notably, the observed correlation between grout pressure and soil displacement can be explained through several interacting mechanisms. When grout is injected at high pressure, the immediate response of the surrounding soil is to form an arch-like structure. This soil arching effect occurs as the soil particles rearrange themselves to redistribute the applied load. In this process, the central zone near the grouting point may experience relatively less displacement because the arch effectively transfers some of the load to the adjacent, more stable soil regions. This mechanism helps in limiting excessive local deformation even when the applied grout pressure is high. The introduction of grout pressure alters the initial stress equilibrium in the soil. As the grout pressure increases, it creates localized zones of high compressive stress near the injection site, which forces the soil to adjust its internal stress distribution. This stress redistribution can result in both compression and tension zones within the soil mass. In areas where the soil yields, plastic deformation may occur, leading to measurable displacements. Conversely, in areas where the soil is still within its elastic limit, the stresses may be redistributed in a way that minimizes further movement. Initially, the mechanical pushing effect of the grout may

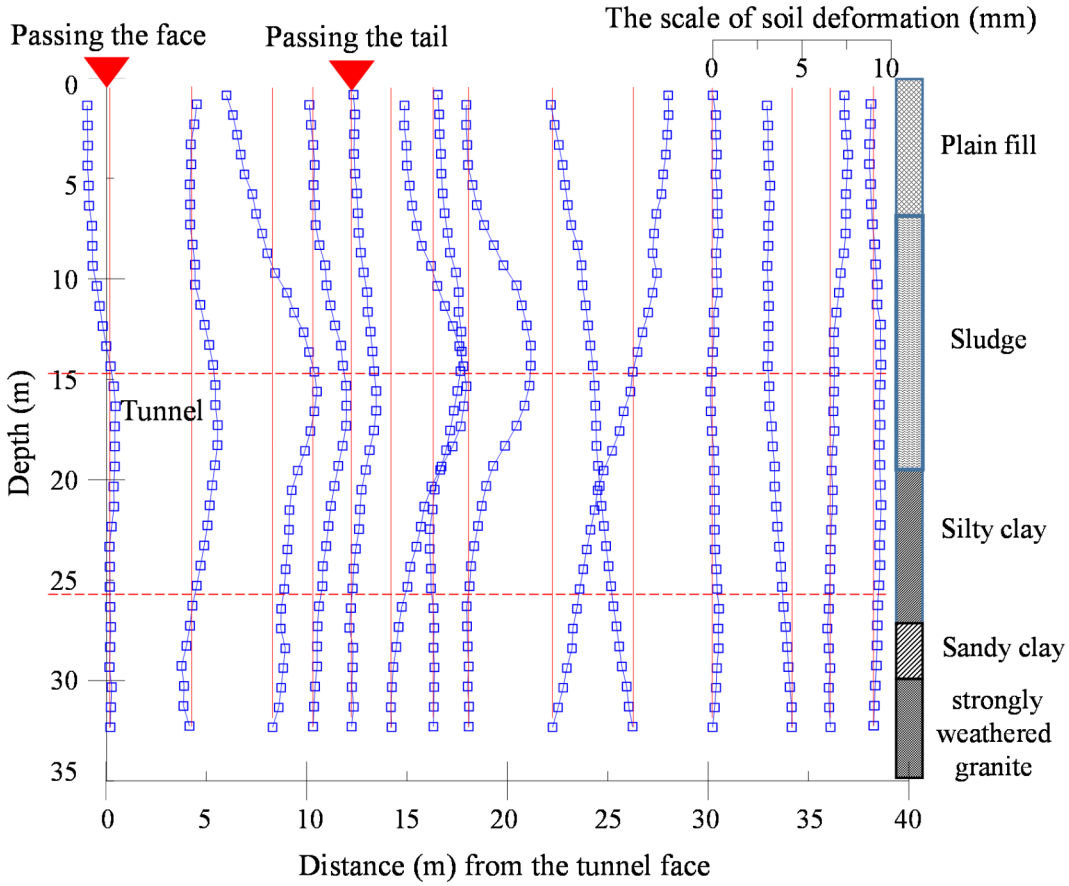

Fig. 7. Lateral horizontal displacement increments at inclinometer tube No. 3. Generated using Grapher 18.

cause the soil to expand or displace outward. However, as the soil arching develops, it counteracts this movement by channeling the loads away from the central region. Concurrently, the stress redistribution further modifies the displacement pattern by creating zones of relative stability and instability. The net result is a complex, non-linear relationship between grout pressure and soil displacement, where the immediate mechanical response is moderated by subsequent arching and stress adjustments.

Analysis of maximum incremental displacements

The analysis was conducted by measuring soil displacements at the same location (i.e., the monitored section) while the shield machine was positioned at varying distances from it. To capture soil disturbance at different longitudinal distances from the shield machine during construction, this study employed the spatial-temporal transformation method[33]. This method is based on the relative movement between the advancing shield machine and the stationary monitored section. It assumes that the soil in the excavation section is homogeneous and that fluctuations in the TBM control parameters have negligible effects on the depth of maximum incremental displacements. By applying this spatial-temporal transformation method, the soil displacements observed at the monitored section for different shield machine positions could be interpreted as the displacements at different longitudinal distances relative to the shield machine's location.

The longitudinal distribution of the lateral horizontal maximum lateral incremental soil displacements, extracted from the incremental curves in Figs. 5, 6, 7 and 8, is presented in Fig. 10. The analysis yielded the following observations: (1) From the midpoint of the shield machine to the shield machine tail (a horizontal width of approximately 0.5D, for which D is the outer diameter of the shield machine), the maximum incremental displacements at the four inclinometer tubes were detected at the depth of the tunnel crown. However, these maximum points showed a downward trend, moving deeper from the midpoint toward the shield machine tail. (2) At the shield machine tail, the maximum incremental displacements occurred at the depth of the shield shoulder, marking the deepest point of displacement during shield construction. (3) Beyond the shield machine tail, as the distance from the tail increased, the depth of maximum incremental displacements became progressively shallower, eventually nearing the ground surface.

In the longitudinal direction, the lateral horizontal disturbance of the surrounding soil induced by synchronous grouting, generally formed a sloped strip. In other words, the lateral horizontal disturbance spread diagonally forward and backward from the grouting pipe. The soil disturbance was concentrated primarily near the shield machine tail. The area ahead of the tail was compartmentalized by the pressure from the mud and water silo (i.e., the cutter head), while the area behind the tail saw propagation toward the surface, where the disturbance

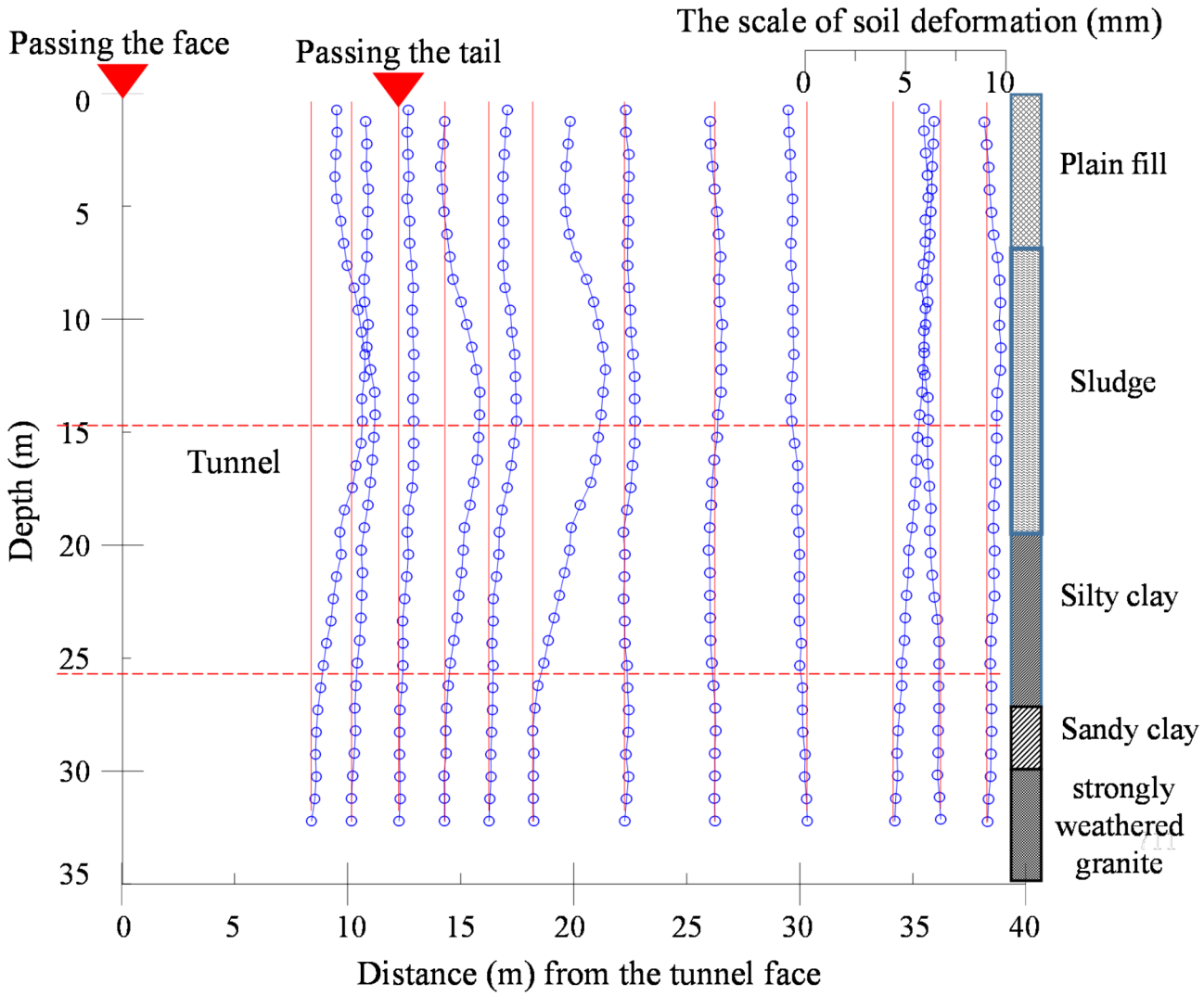

Fig. 8. Lateral horizontal displacement increments at inclinometer tube No. 4. Generated using Grapher 18.

eventually became negligible. The vertical width of the V-shaped disturbance strip was approximately 1D, with its lowest point located near the tunnel shoulder. The inclination angle of the disturbance strip was approximately 39°, close to the passive soil rupture angle (39.3°).

A comparison of data from the various inclinometer tubes in Fig. 10 showed a clear trend that the depth of maximum incremental displacements gradually decreases as the distance from the tunnel increases. The deepest maximum incremental displacement was observed at inclinometer tube No. 1, while the shallowest occurred at inclinometer tube No. 4. This phenomenon indicated that the soil disturbance induced by synchronous grouting also spreads diagonally upward in the lateral direction of the tunnel.

The maximum incremental displacements relative to their positions were compiled and presented in Fig. 11. A discernible trend emerged, indicating that the primary zone of soil disturbance induced by synchronous grouting was predominantly located at positions slightly above the tunnel shoulder when the shield machine tail traversed the monitored section, which spanned from 0.3 m to 22.3 m. A comparison of the maximum incremental displacements on either side of the tunnel revealed a high degree of symmetry. The vertical extent of maximum incremental displacements was concentrated within an approximate range of 0.7D in the depth direction. Laterally, as the distance from the tunnel increased, the positions of maximum incremental displacements gradually ascended, ultimately approaching the surface. Furthermore, the boundary delineations of the main disturbed soil area were essentially horizontal for soil in close proximity to the tunnel, whereas the slope of these boundaries increased progressively with distance from the tunnel.

As previously described, the lateral horizontal area of soil disturbance induced by synchronous grouting exhibited distinct characteristics: (1) in the longitudinal direction of the tunnel, the lateral horizontal maximum incremental displacements were distributed in a V-shaped pattern (as illustrated in Fig. 10); (2) in the lateral direction of the tunnel, the lateral horizontal maximum incremental displacements primarily occurred at positions slightly above the tunnel shoulder and subsequently shifted upward with increasing distance from the tunnel, resulting in a symmetrical disturbance area with a gentle slope that steepened further away (as depicted

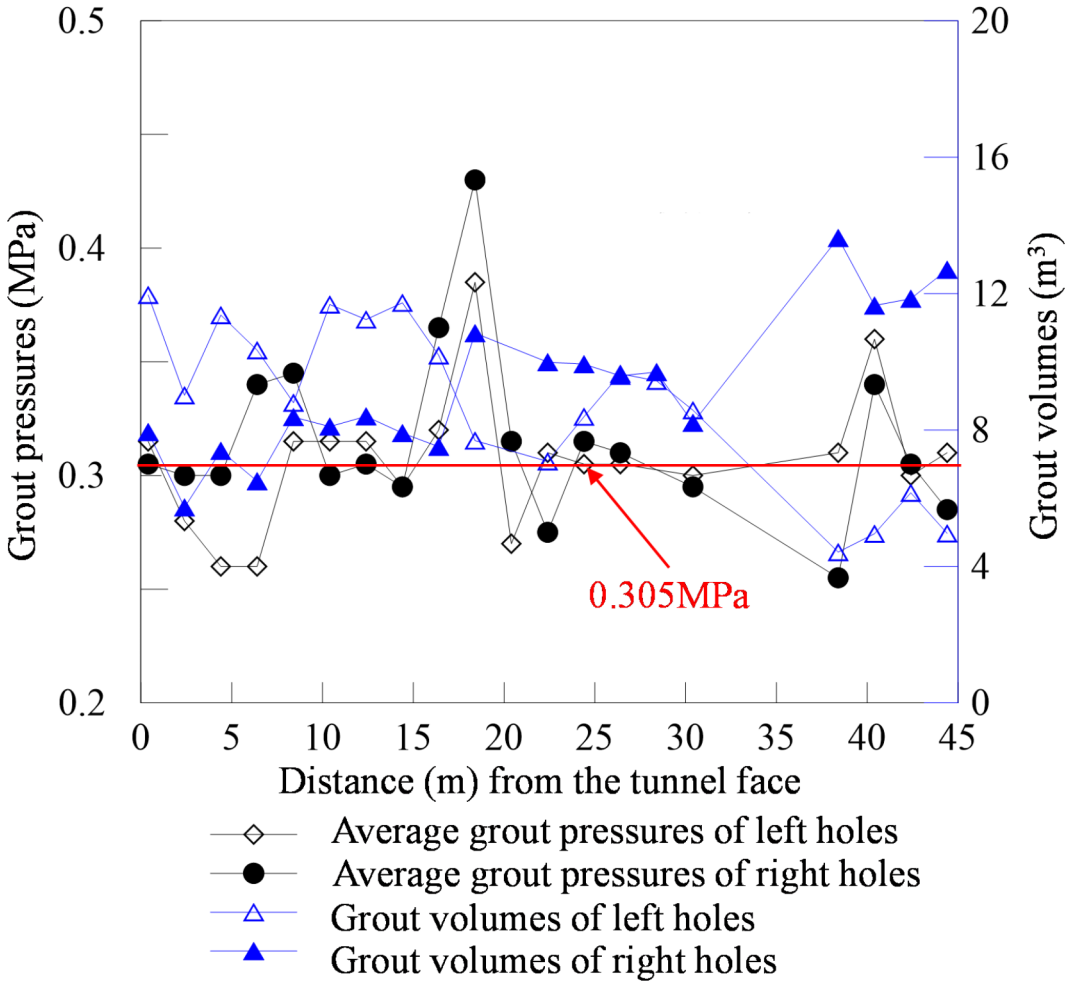

Fig. 9. Grout volumes and average grout pressures during shield advancement on two sides of the monitored section. Generated using Grapher 18.

in Fig. 11). To effectively mitigate the passive impact of synchronous grouting on surrounding structures, careful monitoring should focus on the stages when the shield machine tail is approaching the target section and immediately after passing through it, specifically within the range of 0.3 m to 22.3 m. Priority protection should be applied to areas slightly above the tunnel shoulder.

Comparison of various cases

The lateral horizontal displacement results from six other projects were extracted and analyzed using the incremental displacement method and then compared with data from the current project, as listed in Table 2. Among these projects, the diameters of cases A and B are 14.93 m and 11.58 m, respectively, with burial depths ranging from approximately 1.7D to 2.6D. Both cases involve large-diameter shield tunnels, making them the most comparable to this study case. The strata encountered in cases C and D were also highly similar, primarily consisting of sandy silt and silty clay, with burial depths close to 2–3D. Figure 12 shows a comparison of the lateral horizontal disturbances along the longitudinal direction of the tunnel based on an analysis of maximum incremental displacements. The following observations were made from this comparison:

(1) For the surrounding soil from the cutter head to a position approximately 1D beyond the shield machine tail, the maximum lateral horizontal incremental displacements were primarily concentrated between the tunnel shoulder and approximately 0.5D above the tunnel crown, forming a V-shaped distribution. This could be due to the restraining effect of shear strength at the boundary of the cutter head[40].
(2) Due to large monitoring intervals in cases A and B and the absence of data on lateral horizontal displacements behind the shield machine tail, a detailed analysis of soil disturbance in that region was not feasible. However, their data indicated that the maximum lateral horizontal incremental displacements near the shield machine tail were minimal and developed with an upward trend, resembling a similar V-shaped distribution that was observed in this study.
(3) Monitored data for case F, for which it was located in moderately to slightly weathered argillaceous siltstone, displayed the greatest dispersion yet al.so exhibited a similar V-shaped distribution. Data from case C clear-

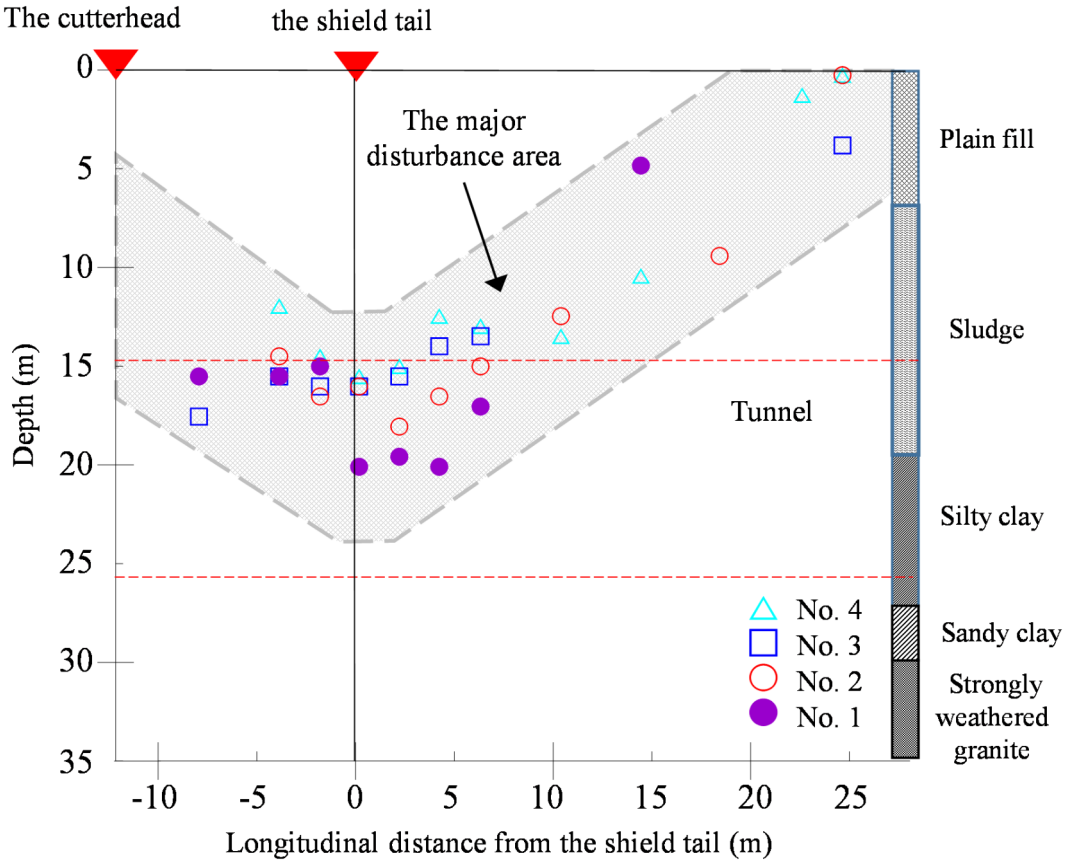

Fig. 10. Longitudinal distribution of lateral horizontal maximum incremental displacements of soil. Generated using Grapher 18.

ly indicated that disturbance was mainly confined to the upper half of the tunnel. Although the limited data due to large monitoring intervals restricted clear observation of consistent patterns, cases D and E1 likewise showed roughly V-shaped trends.

Figure 13 presents a comparison of lateral horizontal disturbances along the tunnel's lateral direction across various cases, based on an analysis of maximum incremental displacements. The following insights were drawn from this comparison:

(1) Lateral horizontal disturbances were primarily observed from the tunnel shoulder up to approximately 0.5D above the tunnel crown, with the main soil disturbance area gradually shifting upward as the distance from the tunnel increased.
(2) In the large-diameter cases (A, B, and C), disturbance distribution was predominantly contained within 1D above the tunnel axis in the vertical direction and within 1.5D to the right of the tunnel axis in the horizontal direction, showing minimal deviation compared to the study case.
(3) Data from cases D, E2, and F were relatively more dispersed. This dispersion is likely due to significant variations in stratigraphic parameters, as the strata in these cases included clay, sand, sludge, and even pebbles. Additionally, case D was located in moderately to slightly weathered siltstone, while case E2 partially intersected a pebble layer. The monitored sections had relatively hard strata, potentially leading to reduced lateral horizontal displacements and maximum incremental displacements. Consequently, the impact of measurement and interpretation errors was amplified, obscuring clear patterns in the maximum incremental displacement data.

Discussion

Deformation modes of the surrounding soil caused by synchronous grouting

Through theoretical analysis of the balance between shield machine tail grouting pressure and the surrounding soil and water pressures, the following behavior pattern from top to bottom is observed: (1) at the tunnel crown, the grouting pressure at the shield machine tail must counterbalance the vertical soil and water pressure at the crown, acting vertically downward; (2) at the tunnel axis depth, specifically at the outermost points on the left and right sides of the tunnel's circular cross-section, the grouting pressure must counteract the horizontal soil pressure at this depth, acting horizontally toward the tunnel axis; (3) at the tunnel base, the grouting pressure counters the upward vertical soil and water pressure; and (4) at the tunnel shoulder and below the axis, the

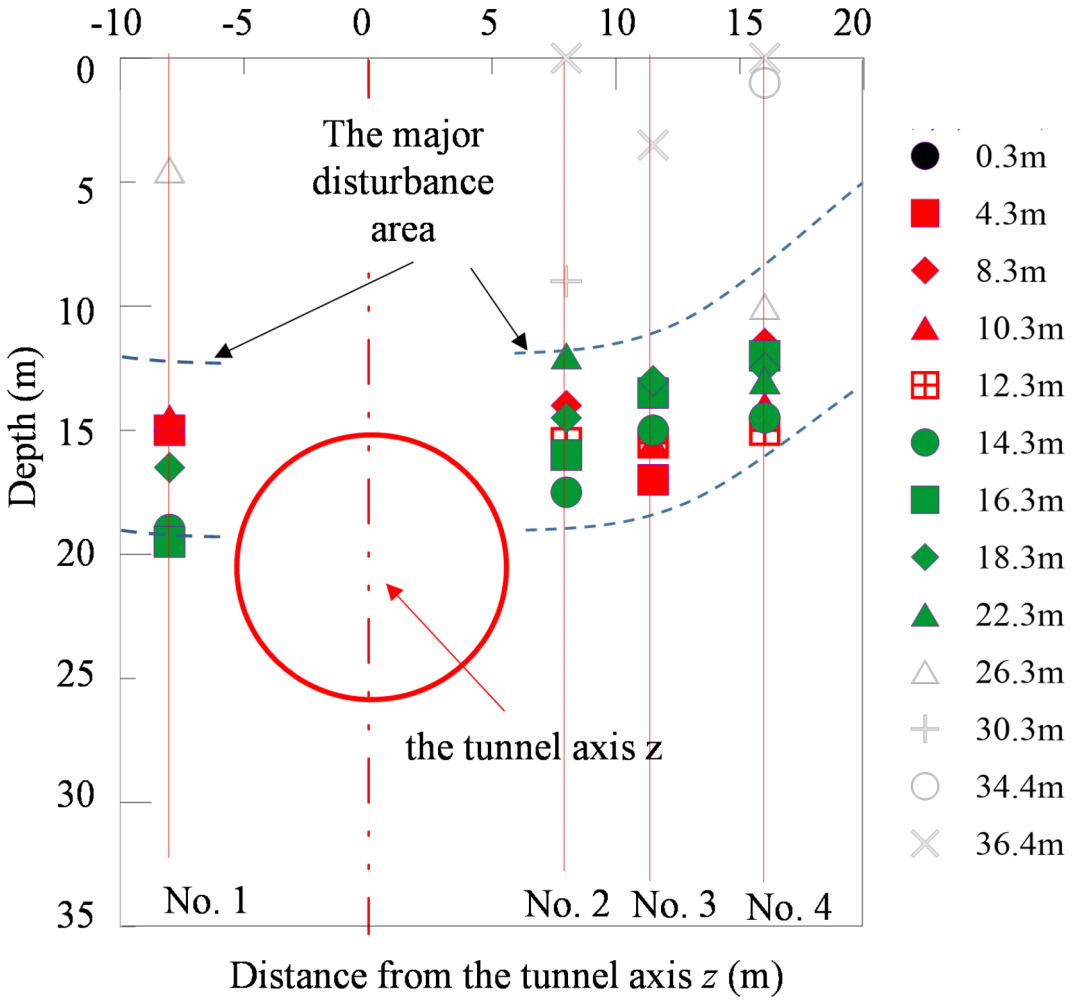

Fig. 11. Distribution of lateral horizontal maximum incremental displacement of soil. Generated using Grapher 18.

Cases	Diameter of the cutter head (m)	Cover depth (m)	The type of shield machine	Geological conditions	Distance of inclinometer tube from tunnel edge (m)	Minimum monitoring interval distance (m)
Study case	11.71	20.4–23.4	Slurry shield	Sludge, silty clay, sandy clay and completely decomposed granite	2.1–16	2
Case A	14.93	25	Slurry shield	Silty clay	2.5–15	7
Case B	11.58	30.5	Slurry shield	Sandy clay and silty clay	6.0–12.0	≈4
Case C	6.34	12.1 ~ 19.2	EPB	Sandy silt and silty clay	1.0–13.7	≈7
Case D	6.34	16.6	EPB	Muddy clay and silty clay	3.1–9.3	≈6
Case E1	6.28	16.4	Slurry shield	Sandy clay, lime sand, clay	1.3–2.5	≈7
Case E2	6.28	13.6	EPB	Reddish brown sludge, clay and pebbles	1.5	≈7
Case F	6.26	29.3	EPB	Moderately to slightly weathered argillaceous siltstone	2.8–16.8	≈5

Table 2. Basic construction parameters of shield tunnel cases. Case A = Shanghai Hongmei South Road Tunnel[34]; Case B = Shanghai Xizang South Road Crossing River Tunnel[35]; Case C = Hangzhou Metro Line 1[36]; Case D = Shanghai Metro Line 2[37]; Case E1 = France Lyon Tunnel, Sect. 1[25]; Case E2 = France Lyon Tunnel, Sect. 2[38]; Case F = Guangzhou Metro Line 2 South Extension[39].

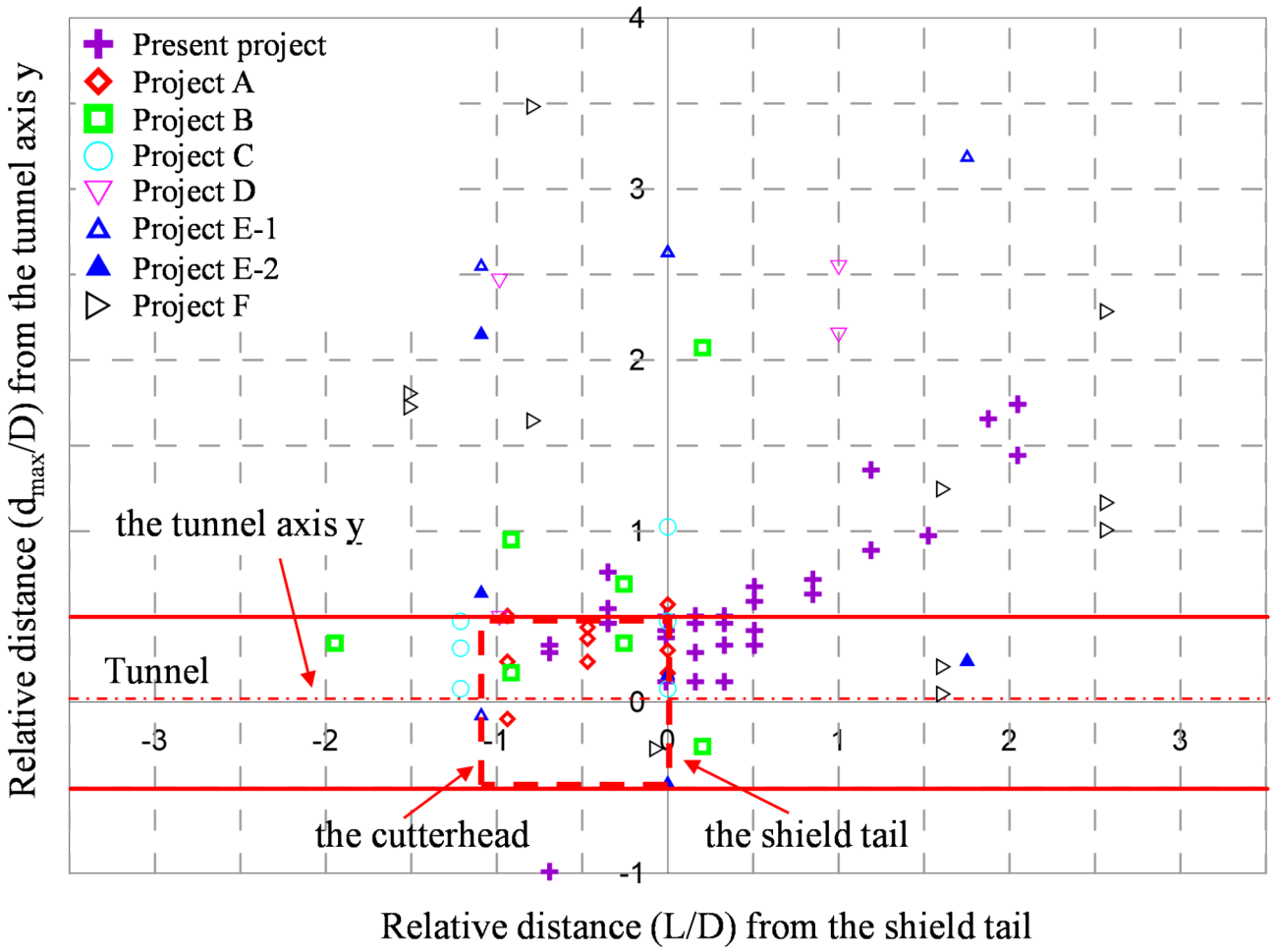

Fig. 12. Comparison of lateral horizontal disturbances along the longitudinal direction between cases. Generated using OriginPro 2022.

pressure acts perpendicular to these points, directed toward the tunnel axis. As the grouting pressure increases, four types of soil deformation patterns emerge around the tunnel, corresponding to these equilibrium conditions.

The injected grout volume affects both the degree of filling within the shield machine tail gap and the resulting soil deformation around the shield machine tail. The following scenarios are likely: (1) if the grout volume is less than the shield machine tail gap, the surrounding soil deforms inward, causing vertical settlement and horizontal inward movement; (2) when the grout volume equals the shield machine tail gap, an initial equilibrium is maintained at the point of injection. However, as water in the grout permeates and the grout hardens and shrinks, the actual grout volume falls below the gap, resulting in delayed soil deformation; (3) when the grout volume slightly exceeds the gap, the surrounding soil experiences slight outward deformation during injection but gradually reverts to its original state over time; and (4) if the grout volume significantly exceeds the gap, it exerts outward pressure on the surrounding soil, causing vertical uplift and horizontal outward expansion.

Based on the analysis of grouting pressure and grout volume, four distinct deformation modes are identified during the shield machine tail arrival and departure stages, which can be described as follows:

DM 1: When the shield machine tail grouting pressure is insufficient to balance vertical and horizontal soil pressures and the grout volume does not fully fill the shield machine tail gap, the surrounding soil undergoes vertical settlement and horizontal inward displacement. The displacement vector for the surrounding soil, illustrated in Fig. 14a, indicates that inward deformation directed toward the tunnel, starting from above the tunnel base. The horizontal inward displacement is most significant near the tunnel shoulders, with soil near the crown experiencing vertical settlement. Additionally, soil near the tunnel shoulders and slightly above exhibits both vertical settlement and horizontal inward movement, resulting in an oblique deformation vector oriented toward the tunnel.

DM 2: When the grouting pressure exceeds the lateral soil pressure but remains below the vertical pressure at the tunnel crown, and the grout volume is approximately equal to the shield machine tail gap volume, the soil above the crown undergoes vertical settlement while the soil on both sides expands outward horizontally, although some soil near the surface shows inward contraction. As depicted in Fig. 14b, the displacement vector at the tunnel crown resembles DM1, but a unique pattern of horizontal outward displacement of deeper soil and horizontal inward contraction near the surface appears on both sides of the tunnel. Dividing the soil into two

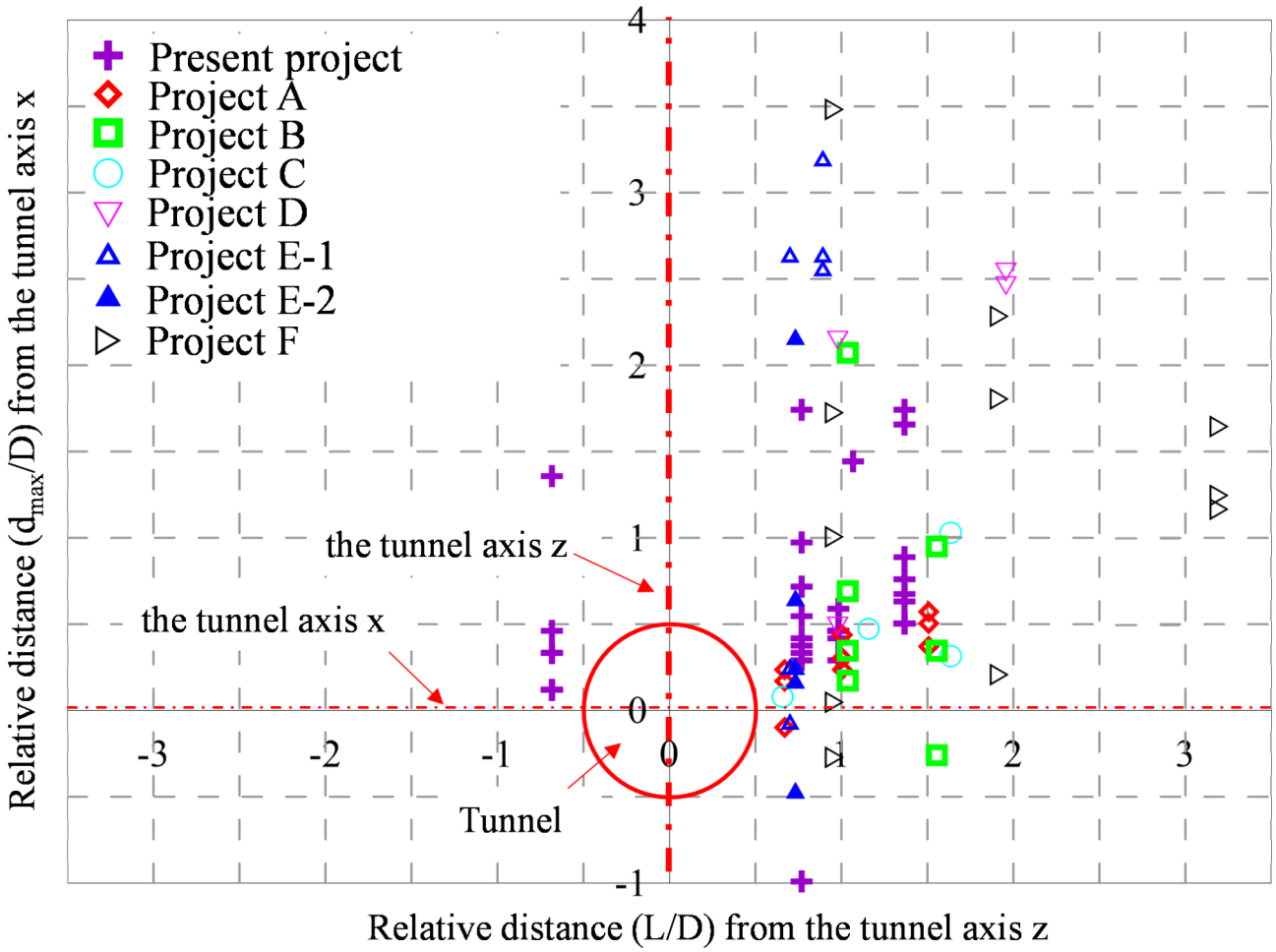

Fig. 13. Comparison of lateral horizontal disturbances along the lateral direction between cases. Generated using OriginPro 2022.

zones based on horizontal contraction (zone ①) and expansion (zone ②), the boundary between these zones originates at the tunnel shoulders and extends diagonally outward. This unique behavior occurs as increased grouting pressure drives soil in zone ① outward horizontally, with displacements greater closer to the tunnel. Meanwhile, at the tunnel crown, the grouting pressure remains below the original vertical stress, causing grout to flow downward under gravity, filling the lower section before reaching the crown and resulting in vertical settlement at the crown and horizontal contraction in zone ②. This phenomenon may lead to a shear plane between zones ① and ②, potentially exerting shear forces on structures crossing this area, such as pipelines or underground pile foundations.

DM 3: As grouting pressure and grout volume increase further, the soil above the tunnel crown experiences vertical settlement, while the soil on both sides undergoes minor uplift and lateral expansion. This mode, illustrated in Fig. 14c, differs from DM2 in that the soil on both sides exhibits slight surface uplift and horizontal expansion, narrowing zone ② symmetrically along the tunnel cross-section axis while expanding zone ①.

DM 4: When grouting pressure is significantly high, the ground surface experiences pronounced uplift, especially along the tunnel axis compared to the sides, and the surrounding soil undergoes notable horizontal expansion. As shown in Fig. 14d, the soil around the tunnel deforms outward from the tunnel, with zone ② fully disappearing. In this scenario, the shield machine tail grouting pressure forces surrounding soil outward and upward, causing the ground surface above the tunnel axis to rise more than at the sides due to its proximity to the tunnel and minimal overlying soil thickness. This results in a pronounced uplift at the weakest points, producing maximum surface deformation. During shield passage and shield machine tail departure, other construction parameters, such as slurry chamber pressure and shield alignment, inevitably affect soil conditions. However, field measurements indicate that soil deformation and stress increments during the early shield passage (e.g., cutterhead entry) are minimal and, therefore, are not analyzed here.

To analyze the mechanisms and timing behind the formation of the four deformation modes, the grouting pressure and volume curves for shield machine tail grouting were plotted as the shield machine tail passed through the test section. These were examined in conjunction with the excess pore water pressure curves at each section. For Sect. 1, as shown in Fig. 15a, deformation modes DM3 and DM4 were primarily observed from 7.2 m before the shield machine tail reached the section to 9.8 m after it passed. It is evident that DM4 occurred

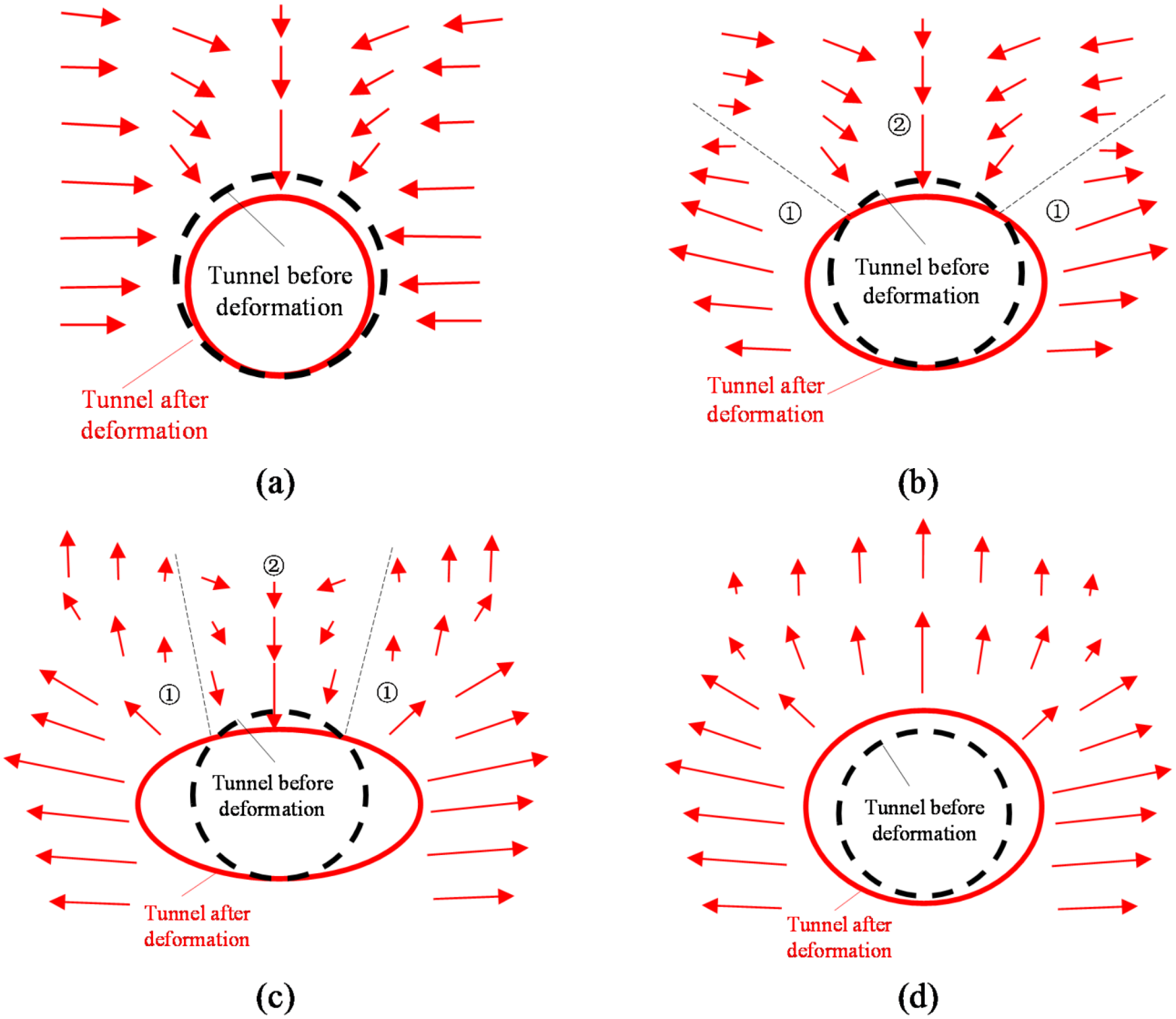

Fig. 14. Schematic diagram of soil displacement vectors around the tunnel under various deformation modes: (**a**) DM 1; (**b**) DM 2; (**c**) DM 3; (**d**) DM 4. (Note: DM (number) represents the deformation mode number) Generated using Visio 2023.

when the grouting pressure was relatively high (approximately 0.32–0.44 MPa), whereas DM3 appeared as the grouting pressure dropped to its lowest level of 0.3 MPa during this stage. Additionally, based on the excess pore water pressure curve measured near the tunnel crown, DM3 was associated with the decline phase of excess pore pressure, while DM4 was observed during the pressure increase phase.

For Sect. 2, as shown in Fig. 15b, all four deformation modes were observed from 3.1 m before the shield machine tail reached the section to 13.1 m after it exited. First, within the range of -3.1 m to -1.1 m, grouting pressure increased while grout volume decreased, leading to DM3. Then, between − 1.1 m and 1.1 m, DM2 appeared as grouting pressure declined and grout volume increased. In the following range of 1.1 m to 3.1 m, both grouting pressure and grout volume decreased, resulting in DM1. Subsequently, from 3.1 m to 9.1 m, increases in both grouting pressure and grout volume led to DM4, although the increments were relatively small. During this period, the pressure slightly decreased and then recovered, while the grout volume reached its peak. Finally, between 9.1 m and 13.1 m, as grout volume decreased, DM1 reappeared. According to the excess pore water pressure curve recorded near the tunnel crown, the excess pore pressure showed a continuous downward trend throughout this process, consistent with the transition from DM3 to DM1.

Causes of the soil lateral upward movement phenomenon

Based on the soil displacement increment curve, representative shield machine tail grouting parameters for specific stages were selected, as listed in Table 3. The grouting behavior of the four grouting ports at the shield machine tail was grouped into left and right sets along the tunnel axis. The average grouting pressure was compared to the static water-soil pressure at the axis and the self-weight stress of water-soil at the tunnel crown.

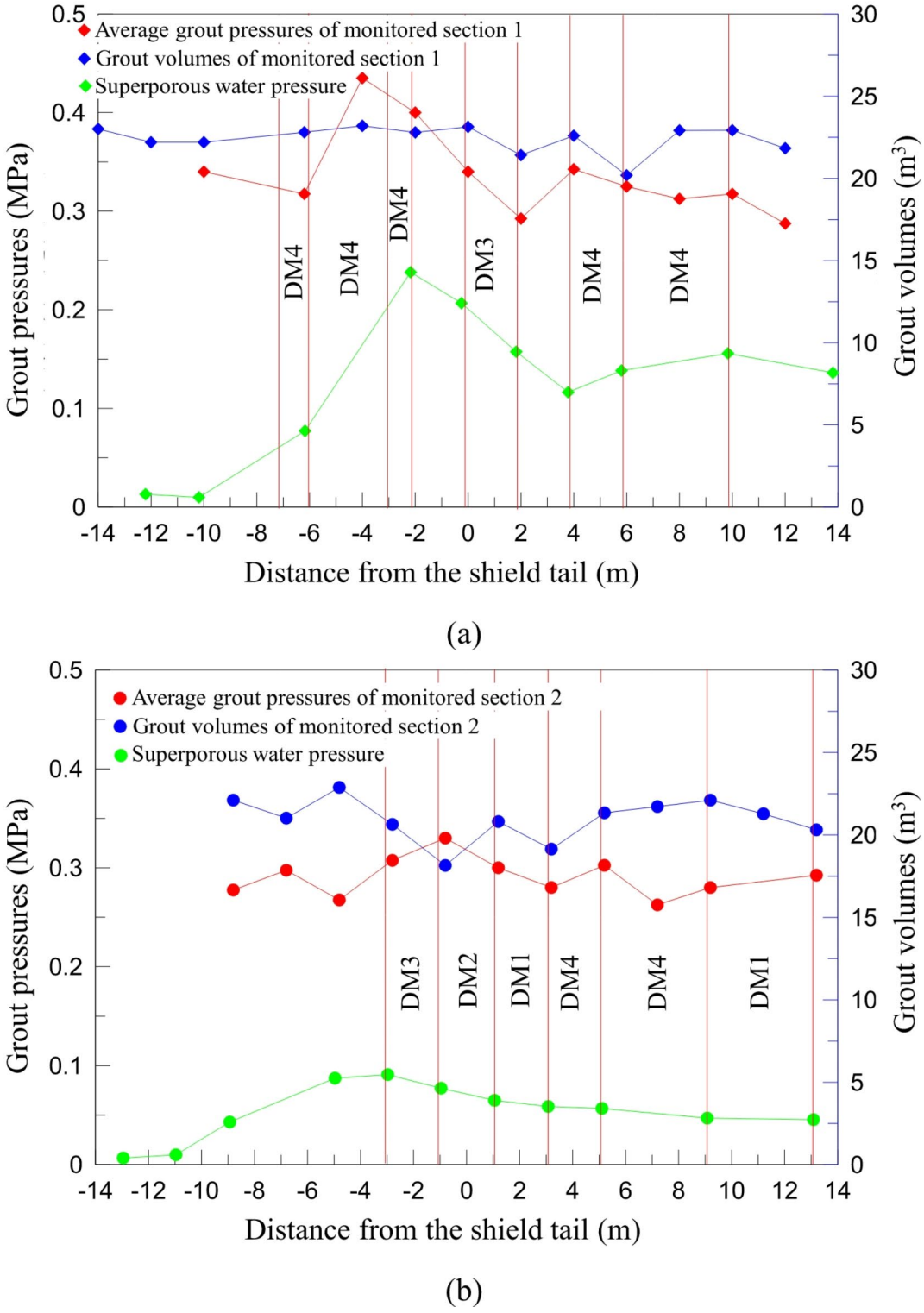

Fig. 15. Grouting pressure, grouting volume and excess pore water pressure curves while the shield machine tail crosses a monitored section: (**a**) Sect. 1; (**b**) Sect. 2. (Note: A positive distance value from the shield machine tail indicates that the monitored section is ahead of the shield machine tail, while a negative value indicates it is behind. (Note: DM (number) represents the deformation mode number during the stages between the red dashed lines) Generated using OriginPro 2022.

Section number	1	2
Distance to the shield machine tail	1.8 m	-1.0 m
Average grout pressures of left holes (MPa)	0.24 (1.20/0.80)	0.30 (1.43/1.00)
Average grout pressures of right holes (MPa)	0.35 (1.75/1.17)	0.36 (1.71/1.20)
Average grout pressures (MPa)	0.29 (1.45/0.97)	0.33 (1.57/1.10)
Grout volumes of left holes (m^3)	16.40	8.75
Grout volumes of right holes (m^3)	6.82	9.40
Total grout volumes in full section (m^3)	21.40	18.15

Table 3. Synchronized grouting parameters of shield machine tail in sects. 1 and 2. The figures in parentheses are the ratio of grouting pressure to the static soil and water pressure at the tunnel axial depth (combined, 0.20 MPa and 0.21 MPa for Sects. 1 and 2, respectively) and the soil and water stress on top of the tunnel (0.30 MPa for Sects. 1 and 2, respectively).

Total grouting volume was taken as the sum of individual volumes. With reference to Fig. 13; Table 3, the analysis reveals the following:

1. At 1.8 m beyond Sect. 1, the average grouting pressure exceeded the static water-soil pressure along the tunnel axis, causing horizontal expansion of the soil on both sides of the tunnel. Compared to the tunnel crown, this relatively low stress resulted in vertical settlement above the tunnel, leading to lateral upward movement. Observing the grouting pressure and volume distribution in Sect. 1, the pressure on the left side is lower than on the right, while the grouting volume is substantially higher on the left. This distribution leads to greater horizontal displacement on the right and slightly higher vertical displacement on the left, suggesting that both factors influence displacement increments around the tunnel.
2. At 1.0 m before reaching Sect. 2, the grouting pressure remained greater than both the lateral water-soil pressure along the axis and the self-weight stress at the tunnel crown. However, the horizontal displacement increment was minimal, and settlement occurred above the tunnel. This could be because the interlocking of the grains was relatively weak due to the size and shape of the interstitial voids[41]; grouting at the shield machine tail primarily flows backward to fill the larger shield machine tail gap, with limited forward flow. Consequently, the soil above the tunnel axis remains influenced by factors like the slurry chamber and the shield's alignment.

In summary, the lateral upward movement phenomenon is primarily caused by grouting pressure exceeding the in-situ static water-soil pressure (by 1.07–1.57 times in this case). The injected grout displaces the soil surrounding the tunnel, forcing it away from the tunnel and diagonally upward, leading to ground uplift on both sides. Due to the large shield machine tail gap at the tunnel crown and the soil's significant self-weight stress, the grouting pressure is insufficient to fully support the vertical soil load, causing downward movement and potentially resulting in reduced uplift or vertical settlement above the tunnel axis. When the self-weight stress of the tunnel crown soil is less than the lateral pressure along the axis, more pronounced bulging above the axis may accompany lateral upward movement. Additionally, grouting volume influences this phenomenon: with similar grouting pressures on both sides, uneven grouting volumes can exacerbate lateral upward movement, with asymmetry in grouting volume leading to asymmetric upward movement.

The occurrence of lateral upward movement indicates that the grouting pressure or volume at the shield machine tail may be excessive, warranting close monitoring during shield construction. This unique deformation phenomenon also suggests that attempts to control surface settlement through shield machine tail grouting may inadvertently cause excessive uplift of the soil on either side of the tunnel, leading to other potential issues. The causes of this phenomenon can be attributed to two primary factors: (1) the grouting pressure at the shield machine tail, which should be calibrated based on the lateral soil pressure at the depth of the tunnel axis as well as the overburden stress at the tunnel crown; and (2) the grouting volume, which directly affects the degree of uplift. Therefore, it is recommended to implement comprehensive monitoring during shield construction to detect and prevent lateral uplift. Additionally, optimization can be achieved through strategic placement of shield machine tail grouting pipes and precise control over grouting pressure and volume, minimizing the risk of such phenomenons.

Summary and conclusions

Through comprehensive monitoring during shield construction and comparison with previous projects, the lateral horizontal displacements of the surrounding soil were carefully analyzed, leading to the following summaries and conclusions:

(1) Compared to analyzing total displacement, examining displacement increments isolates the effects of each construction phase by removing cumulative impacts from previous processes, providing a clearer view of each step's influence on the surrounding soil. Incremental displacement analysis indicated that synchronous grouting primarily caused outward deformation in the lateral direction. During shield machine passage, the main disturbed area showed a pattern of descending toward the tunnel shoulder before rising back toward the surface.

(2) The maximum incremental displacement method was developed in this study incorporating incremental displacement and spatiotemporal transformation techniques, revealing patterns in soil disturbance near the shield machine tail along both longitudinal and lateral axes. In the longitudinal direction, maximum lateral horizontal displacement increments showed a V-shaped distribution, approximately 1D in width, with the lowest point near the tunnel shoulder. The perimeter of the V-shaped area closely matches the passive rupture angle of the soil. In the lateral direction, the primary disturbance area from synchronous grouting, symmetrical on both sides of the tunnel, was located slightly above the tunnel shoulder with a vertical width of about 0.7D. Furthermore, as the distance from the tunnel increased, the location of maximum displacement increment areas also rose.
(3) Displacement data processed with analysis of maximum incremental displacements from several other cases produced results consistent with those observed in this study, particularly in projects involving relatively soft strata. To mitigate the impact of synchronous grouting on nearby structures during shield construction, attention should focus on stages when the shield machine tail is close to passing the target section. Priority protection should be provided to the area just above the tunnel shoulders to safeguard surrounding structures effectively.

Data availability

Data will be made available from the corresponding author upon reasonable request.

Received: 21 January 2025; Accepted: 24 February 2025
Published online: 07 April 2025

References

1. Zeng, B. & Huang, D. Soil deformation induced by Double-O-Tube shield tunneling with rolling based on stochastic medium theory. *Tunn. Undergr. Space Technol.* **60**, 165–177 (2016).
2. Li, H., Li, X. & Liu, H. Deformation and failure mechanism of metro shield tunnel subjected to buried fault dislocation. *Eng. Fail. Anal.* **153**, 107551 (2023).
3. Wang, T., Geng, P., Li, P., Wang, Q. & Wang, L. Deformation and failure of overburden soil subjected to normal fault dislocation and its impact on tunnel. *Eng. Fail. Anal.* **142**, 106747 (2022).
4. Chen, X., Hu, Y., Zhang, L. & Liu, Y. 3D large-deformation modelling on face instability and sinkhole formation during tunnelling through non-uniform soils. *Tunn. Undergr. Space Technol.* **134**, 105011 (2023).
5. Du, X., Li, Y., Dong, X. & Han, K. Large deformation induced soil pressure changes in a loess tunnel. *Eng. Fail. Anal.* **163**, 108568 (2024).
6. Fang, K. et al. Insights into the deformation and failure characteristic of a slope due to excavation through multifield monitoring: a model test. *Acta Geotech.* **18** (2), 1001–1024 (2023).
7. Peck, R. B. Deep excavations and tunnelling in soft ground, *Int. Conf. Soil Mech. Found. Eng.*, Mexico, (1969).
8. Celestino, T. B., Gomes, R. A. M. P. & Bortolucci, A. A. Errors in ground distortions due to settlement trough adjustment. *Tunn. Undergr. Space Technol.* **15**, 97–100 (2000).
9. Hu, X. Y., He, C. A., Peng, Z. Z. & Yang, W. B. Analysis of ground settlement induced by Earth pressure balance shield tunnelling in sandy soils with different water contents. *Sustain. Cities Soc.* **45**, 296–306 (2019).
10. Jin, Y. et al. Mechanical and macro-microscopic failure characteristics of Grouted mudstone considering Grout dehydration effect. *Eng. Fail. Anal.* **142**, 106662 (2022).
11. Peng, S., Luo, J., Luo, G., Cao, H. & Pan, H. Laboratory modeling on sand erosion by tunnel leakage in water-rich sand strata. *Acta Geotech.* **19**, 8089–8110 (2024).
12. Ying, K. et al. Backfill grouting diffusion law of shield tunnel considering porous media with nonuniform porosity. *Tunn. Undergr. Space Technol.* **127**, 104607 (2022).
13. Liang, J., Cui, J., Lu, Y., Li, Y. & Shan, Y. Limit analysis of shallow tunnels collapseproblem withoptimizedsolution. *Appl. Math. Model.* **109**, 98–116 (2022).
14. Peng, S. et al. Failure mechanisms of ground collapse caused by shield tunnelling in water-rich composite sandy stratum: A case study. *Eng. Fail. Anal.* **146**, 107100 (2023).
15. Guo, P., Gong, X., Wang, Y., Lin, H. & Zhao, Y. Analysis of observed performance of a deep excavation straddled by shallowly buried pressurized pipelines and underneath traversed by planned tunnels. *Tunn. Undergr. Space Technol.* **132**, 104946 (2023).
16. Lavasan, A. A. et al. Numerical investigation of tunnelling in saturated soil: the role of construction and operation periods. *Acta Geotech.* **13**, 671–691 (2018).
17. Liu, X., Chen, H., Liu, Q., Liu, B. & He, J. Modelling slurry flowing and analyzing grouting efficiency under hydro-mechanical coupling using numerical manifold method. *Eng. Anal. Bound. Elem.* **134**, 66–78 (2021).
18. Wang, Y. et al. Simplified analytical solutions for tunnel settlement induced by axially loading single pile and pile group. *J. Eng. Mech.* **147**, 04021116 (2021).
19. Luo, G. et al. Modelling initiation stage of backward erosion piping through analytical models. *Land* **12**, 1970 (2022).
20. Li, Y. et al. Seismic performance study of immersed tunnel with longitudinal limit device of flexible joint. *Undergr. Space*. **20**, 17–32 (2025).
21. Broere, W. & Festa, D. Correlation between the kinematics of a tunnel boring machine and the observed soil displacements. *Tunn. Undergr. Space Technol.* **70**, 125–147 (2017).
22. Mair, R. J. & Taylor, R. N. Bored tunnelling in the urban environment, *Int. Conf. Soil Mech. Found. Eng.*, Hamburg, Germany, (1997).
23. Zhou, J. et al. Prediction ofthe seismicbehavior and backfillingscheme optimization of immersed tunnel based on the Ruyifang project. *Soil. Dyn. Earthq. Eng.* **37**, 1114–1119 (2017).
24. Cao, L., Chen, X., Lu, D., Zhang, D. & Su, D. Theoretical prediction of ground settlements due to shield tunnelling in multi-layered soils considering process parameters. *Undergr. Space*. **16**, 29–43 (2024).
25. Peng, S. & Rice, J. D. Inverse analysis of laboratory data and observations for evaluation of backward erosion piping process. *J. Rock. Mech. Geotech. Eng.* **12**, 1080–1092 (2020).
26. Wu, D. et al. Ground deformation characteristics induced by mechanized shield twin tunnelling along curved alignments. *Adv. Civ. Eng.* **2021** (1), 6640072 (2021).
27. Wang, W., Cui, J., Shan, Y., Li, Y. & Hou, Z. Numerical analysis of slurry flow in pile-end grouting of the drilling with prestressed concrete pipes. *Struct. Concrete*. **24**, 7237–7248 (2023).
28. Loganathan, N. Analytical prediction for tunnelling induced ground movements in clays. *J. Geotech. Geoenviron Eng.* **124**, 846–856 (1998).

29. Park, K. H. Elastic solution for tunnelling-induced ground movements in clays. *Int. J. Geomech.* **4**, 310–318 (2004).
30. Lee, K., Rowe, R. K. & Lo, K. Subsidence owing to tunnelling. I. Estimating the gap parameter. *Can. Geotech. J.* **29**, 929–940 (1992).
31. Rowe, R., Lo, K. & Kack, G. A method of estimating surface settlement above tunnels constructed in soft ground. *Can. Geotech. J.* **20**, 11–22 (1983).
32. Cao, L. Q., Zhang, D. L., Fang, Q. & Yu, L. Movements of ground and existing structures induced by slurry pressure-balance tunnel boring machine (SPB TBM) tunnelling in clay. *Tunn. Undergr. Space Technol.* **97**, 103278 (2020).
33. Pan, Z. Study on soil disturbance and its classified settlement due to EPB TBM excavation, China Univ. Mining Technol.-Beijing, Beijing, China (in Chinese), Ph.D. thesis (2016).
34. Zhou, X. L. The interaction between two super-close tunnels constructed by extra large diameter slurry shield, Univ. Shanghai Sci. Technol., China (in Chinese), Ph.D. thesis (2013).
35. Du, J. L., Huang, X. C. & Wang, F. Measurement and simulation of subsoil disturbance of large section slurry shield construction. *Chin. J. Undergr. Space Eng.* **5**, 1205–1210 (2009). (in Chinese).
36. Yu, X. F., Ren, H. & Hu, X. D. Analysis of the disturbance to surrounding soils during shield driving for the Hangzhou metro line 1 project. *Mod. Tunn. Technol.* **51**, 166–173 (2014).
37. Lee, K., Ji, H., Shen, C., Liu, J. & Bai, T. Ground response to the construction of Shanghai metro tunnel-line 2. *Soils Found.* **39**, 113–134 (1999).
38. Emeriault, F., Breysse, D., Kastner, R. & Denis, A. Geotechnical survey and mechanical parameters in urban soils: modelling soil variability and inferring representative values using the extension of Lyon subway line D as a case study. *Can. Geotech. J.* **41**, 773–786 (2004).
39. Jia, Y. Ground deformation measurement and three-dimensional numerical simulation and parametric analysis by shield driven, Tianjin Univ., China (in Chinese), Ph.D. thesis (2009).
40. Peng, S. et al. Laboratory investigation effects of blanket defect size on initiation of backward erosion piping. *J. Geotech. Geoenviron Eng.* **150**, 04024095 (2024).
41. Peng, S. & Rice, J. D. Measuring critical gradients for soil loosening and initiation of backward erosion-piping mechanism. *J. Geotech. Geoenviron Eng.* **146**, 04020069 (2020).

Acknowledgements

The research work described herein was funded by the National Natural Science Foundation of China (No. 52308353) and Natural Science Foundation of Guangdong Province (Nos. 2023A1515011571, 2023A1515011683).

Author contributions

S.P.: Writing – original draft, Visualization, Methodology, Conceptualization, Investigation, Formal analysis, Funding acquisition. H.H.: Writing – original draft, Formal analysis, Investigation, Data curation. H.P.: Writing – review & editing, Methodology, Investigation, Conceptualization. G.L.: Writing – review & editing, Conceptualization, Formal analysis, Funding acquisition. H.C.: Writing – review & editing, Supervision.

Declarations

Competing interests

The authors declare no competing interests.

Additional information

Correspondence and requests for materials should be addressed to H.P. or G.L.